ATF3 Reprograms the Bone Marrow Niche in Response to Early Breast Cancer Transformation

Milena Perrone[1], Claudia Chiodoni[1], Mara Lecchi[2], Laura Botti[1], Barbara Bassani[1], Annamaria Piva[1], Elena Jachetti[1], Matteo Milani[1], Daniele Lecis[1], Elda Tagliabue[3], Paolo Verderio[2], Sabina Sangaletti[1], and Mario P. Colombo[1]

ABSTRACT

Cancer is a systemic disease able to reprogram the bone marrow (BM) niche towards a protumorigenic state. The impact of cancer on specific BM subpopulations can qualitatively differ according to the signals released by the tumor, which can vary on the basis of the tissue of origin. Using a spontaneous model of mammary carcinoma, we identified BM mesenchymal stem cells (MSC) as the first sensors of distal cancer cells and key mediators of BM reprogramming. Through the release of IL1B, BM MSCs induced transcriptional upregulation and nuclear translocation of the activating transcription factor 3 (ATF3) in hematopoietic stem cells. ATF3 in turn promoted the formation of myeloid progenitor clusters and sustained myeloid cell differentiation. Deletion of *Atf3* specifically in the myeloid compartment reduced circulating monocytes and blocked their differentiation into tumor-associated macrophages. In the peripheral blood, the association of *ATF3* expression in $CD14^+$ mononuclear cells with the expansion $CD11b^+$ population was able to discriminate between women with malignant or benign conditions at early diagnosis. Overall, this study identifies the IL1B/ATF3 signaling pathway in the BM as a functional step toward the establishment of a tumor-promoting emergency myelopoiesis, suggesting that ATF3 could be tested in a clinical setting as a circulating marker of early transformation and offering the rationale for testing the therapeutic benefits of IL1B inhibition in patients with breast cancer.

Significance: Bone marrow mesenchymal stem cells respond to early breast tumorigenesis by upregulating IL1B to promote ATF3 expression in hematopoietic stem cells and to induce myeloid cell differentiation that supports tumor development.

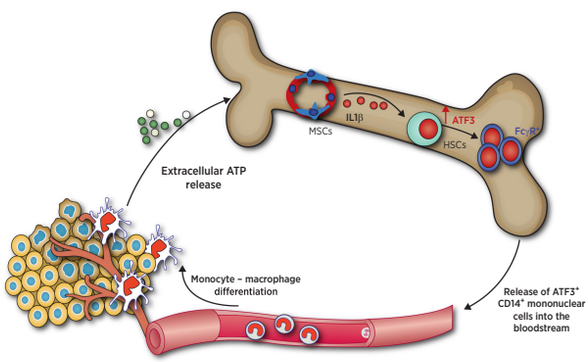

Breast cancer cells reprogram the bone marrow stroma to increase ATF3 activation in hematopoietic stem cells sustaining their differentiation towards $CD14^+ATF3^+$ monocytes.

Introduction

Chronic and acute immune stimulations such as infection, trauma, autoimmunity, and tumors generate a hematopoietic demand that is sensed by the bone marrow (BM) mesenchymal stem cells (MSC). Indeed, the modulation of MSC activity influences lineage differentiation of hematopoietic stem cells (HSC) reprogramming the BM niche to sustain the new hematopoietic spur. In this context, we have previously shown that chronic immune stimulation mimicking lupus-like autoimmunity modifies the BM extracellular matrix (ECM) composition, inducing downregulation of secreted protein acidic and rich in cysteine (SPARC) and collagen-I also subverting the BM tolerogenic microenvironment (1), a condition that induces pathologic myeloproliferation if applied to preleukemic mice (2).

In the case of neoplastic conditions, tumor-derived factors educate the BM stromal compartment to support the expansion of myeloid cells that sustain tumor growth and metastasis, also suppressing immune cell responses (3–6). A feature of this tumor-induced emergency myelopoiesis is the development of GMP clusters, which are induced in the BM by stromal-derived signals, particularly IL1B (7–9). Using a spontaneous model of mammary carcinoma (MMTV-NeuT, NeuT hereafter), we demonstrated that an incipient tumor was able to promote detectable BM stromal changes, which, in our model, consisted in the down-modulation of ECM proteins and up-modulation of the CXCL12/CXCR4 axis, suggesting that stromal rearrangements of the BM niche could represent a very initial step during mammary transformation (10). The gene expression profile (GEP) analysis performed on total BM cells at different stages of transformation highlighted activating transcription factor 3 (*Atf3*) among the top up-modulated genes in the BM of NeuT mice at a preinvasive stage of disease. Its expression in immature cells of the BM such as common myeloid progenitors

[1]Molecular Immunology Unit, Department of Research, Fondazione IRCCS Istituto Nazionale dei Tumori, Milan, Italy. [2]Bioinformatics and Biostatistics Unit, Department of Applied Research and Technological Development, Fondazione IRCCS Istituto Nazionale dei Tumori, Milan, Italy. [3]Molecular Targeting Unit, Department of Research, Fondazione IRCCS Istituto Nazionale dei Tumori, Milan, Italy.

S. Sangaletti and M.P. Colombo contributed equally as co-last authors of this article.

Corresponding Authors: Mario P. Colombo, Fondazione IRCCS Istituto Nazionale dei Tumori, Via Amadeo 42, 20133, Milan, Italy. Phone: 223-902-252; Fax: 223-902-630; E-mail: mariopaolo.colombo@istitutotumori.mi.it; and Sabina Sangaletti, sabina.sangaletti@istitutotumori.mi.it

Cancer Res 2023;83:117–29

doi: 10.1158/0008-5472.CAN-22-0651

(CMP) suggested the involvement of this transcription factor in the regulation of HSC skewing toward the myeloid cell lineage, particularly monocytes (11). In line with this notion, ATF3 overexpression in BM cells limits neutrophil development (12). Despite these pieces of evidence, little is still known about the molecular mechanisms promoting ATF3 activation in the BM niche and its role in driving cancer-adapted myelopoiesis.

In this work, we demonstrate that IL1B released by tumor-primed BM-MSCs induces ATF3 activation in the HSCs and promotes the formation of myeloid progenitor clusters, a necessary step toward myeloid cell differentiation. The cross-talk between distant tumors and the BM ultimately leads to a release of tumor promoting *ATF3*-expressing myeloid cells into the circulation, which were also detected in the peripheral blood (PB) of patients with breast cancer. Notably, the evaluation of *ATF3*-expressing myeloid cells can be used to discriminate among patients with malignant versus benign disease, not clearly defined at radiographic examination.

Materials and Methods

Animal studies

All animal studies and technical procedures, executed in accordance with National Law (D.Lgs 26/2014), were approved by the Institutional Committee for Animal Welfare and by the Italian Ministry of Health (Authorization number 443/2016-PR; 548/2019-PR; 297/2020-PR). MMTV-NeuT (NeuT, BALB/c background) female mice were sacrificed at 12 and 24 weeks of age, two time points representing preinvasive and invasive stages of mammary transformation, respectively (10, 13, 14). Aged-matched control BALB/c mice were used as wild-type counterparts.

The PyMT41c mouse mammary cancer cell line, obtained in our laboratory starting from transgenic MMTV-PyMT mice (C57BL/6 background; ref. 15), was used as transplantable models. The PyMT41c and the PyMT41c-NPMc+ cell line (overexpressing the mutated human NPMc protein able to induce CD8-mediated T-cell responses; ref. 16) were injected in the mammary fat pad of $Atf3^{fl/fl}$LysMCre$^{+/-}$ mice (C57BL/6 background), carrying a specific deletion of the ATF3 in the myeloid compartment, and in $Atf3^{fl/fl}$ control mice.

Cell lines are routinely checked for *Mycoplasma* negativity using MycoAlert Mycoplasma Detection Kit (Lonza). *Mycoplasma* test is usually performed at time of thawing before using cells *in vivo* or for *in vitro* experiments.

Experiments with chronic lipopolysaccharide (LPS) administration were performed in female BALB/c mice, purchased from Charles River Laboratories. Mice were injected intraperitoneally with 10 ug of LPS (O111:B4, Sigma-Aldrich) or PBS, 3 times per weeks for 4 weeks (chronic administration) and sacrificed the day after the last treatment.

Anti-IL1B neutralizing antibody (B122, BioXCell) and relative isotype control (Hamster IgG, BioXCell) were used for *in vivo* studies. The B122 monoclonal antibody was injected in NeuT mice starting from 12 weeks of age. C57BL/6 mice started anti-IL1B treatment 3 days after the injection of the PyMT41c tumor-cell line. In both mouse models, mice were treated two times a week for 4 weeks with anti-IL1B and relative isotype control. Antibodies were injected intraperitoneally with a dose of 50 μg per mouse in 200 uL of physiologic saline solution.

Key research resource

All key research resource used in this work are listed in the key resource table included in the Supplementary Materials and Methods.

Flow cytometry and cell sorting

Femurs of mice were used to obtain BM fresh cells for flow cytometry analysis and cell sorting. Single-cell suspensions were incubated with specific antibodies and acquired using a BD LSRFortessa Flow Cytometer. Progenitors and myeloid cells were sorted with a FACSAria BD instrument.

Multiparametric flow cytometry analysis on PB mononuclear cells (PBMC) was performed using the BD FACSCelesta Flow Cytometer. Monocytes were isolated from the PBMCs using CD14$^+$ MicroBeads human (Miltenyi Biotec) according to the manufacturer's instructions.

Analyses were performed with FlowJo software (version 10.4.2).

Confocal microscopy analysis

Immunofluorescence analyses were performed on frozen OCT-embedded BM samples. For ATF3 intracellular staining, 4-μm thick sections were fixed with 4% paraformaldehyde and permeabilized with 0.1% Triton X-100. For cell membrane staining, sections were fixed with cold acetone. Sections were blocked in PBS1X with 5% BSA and incubated with primary antibody for 2 hours and secondary antibody for 30 minutes. Anti-rat and anti-rabbit (Alexa Fluor 633- and 555-conjugate) secondary antibodies were used for fluorescence detection (Life Technologies). Nuclei were counterstained with the 4′,6-diamidino-2-phenylindole (DAPI) stain. All confocal microscopy analyses were performed using a Leica TCS-SP8-X confocal laser scanning microscope.

Immunostaining analysis

Four-micrometer thick tissue sections of tumors were deparaffinized, rehydrated, and unmasked using Novocastra Epitope Retrieval Solutions in a thermostatic bath at 95°C for 15 minutes. Next, the sections were brought to room temperature and washed in PBS. After neutralization of the endogenous peroxidase with H_2O_2 and Fc blocking by a specific protein solution, samples were incubated overnight with primary antibodies overnight at 4°C. Staining was revealed using IgG (H&L) specific secondary antibodies (Life Technologies) and 3–3′ diaminobenzidine chromogenic substrate. The slides were counterstained with Harris hematoxylin (Novocastra). Sections were analyzed using a Leica DM4 B optical microscope equipped with a Leica DFC450 digital camera.

Isolation of hematopoietic and MSCs from the BM

HSCs were isolated from the BM of mice by immunomagnetic beads (Lineage Cell Depletion Kit, Miltenyi Biotec). Cell suspension was expanded in StemSpan SFEM medium (STEMCELL Technologies) supplemented with SCF (50 ng/mL), TPO (15 ng/mL), IL3 (30 ng/mL), FLT3 ligand (50 ng/mL), and IL6 (20 ng/mL).

MSCs were purified from the bone and the trabecular fraction. Initially cells were incubated with collagenase I (Sigma-Aldrich; 1 mg/mL) for 1 hour at 37°C. Then, cell suspension was incubated with the following PE-conjugated antibody: CD45, B220, CD3, CD11b, CD11c, Gr1, F4/80, Ter119 (all markers of hematopoietic cells). After separation with anti-PE microbeads (Miltenyi Biotec), MSCs were phenotypically characterized by flow cytometry analysis with the following markers: CD45, Ter119, CD31, Sca-1, CD29, CD44.

For *in vitro* experiments, BM-derived mesenchymal cells were expanded and differentiated with MesenCult MSC Basal Medium supplemented with Mesenpure cocktail (STEMCELL Technologies).

HSCs were stimulated for 24 hours with 25 ng/mL of recombinant IL1B (211–11B, PeproTech). Anti-IL1B neutralizing antibody (B122,

BioXCell) and relative Isotype control (Hamster IgG, BioXCell) were added to the medium prior to coculture experiments at the dose of 5 ug/mL. HSCs were also differentiated toward monocytes in the presence of macrophage colony-stimulating factor (M-CSF; 40 ng/mL).

RNA extraction and gene expression analysis

RNA was extracted from cells using Direct-zol RNA Microprep Kit (ZymoResearch) following the manufacturer's instruction and quantified with NanoDrop2000/2000c Spectrophotometers (Thermo Fisher).

For qPCR, RNA was reverse transcribed with SuperScript IV VILO Master Mix with exDNase Enzyme or with High-Capacity cDNA Reverse Transcription Kit. qPCR was performed with ABU Prism 7900 HT (AB) using the TaqMan Fast Advanced PCR MasterMix (Applied Biosystem). Gene expression levels were normalized with β-actin expression (see Supplementary Material and Methods for list of oligonucleotides).

Microarray analysis was performed with Clariom S Assay, mouse (Thermo Fisher). Raw data were preprocessed using the sst-RMA algorithm implemented in the Transcriptome Analysis Console software (Thermo Fisher) and analyzed using R software. Differentially expressed genes were identified using the limma package (17). *P* values were adjusted for multiple tests using the Benjamini–Hocheberg FDR. Functional overrepresentation analysis of differentially expressed genes was carried using the topGO package with Gene Ontology (GO) biological process terms, and Qiagen's Ingenuity Pathway Analysis (IPA, Qiagen).

Graph and statistical analysis

As regards *in vitro* and *in vivo* experiments:

- Descriptive statistical analysis was performed reporting means with SD in the graphical representations of data.
- Differences between groups of interest were assessed through the nonparametric Permutation (P), or Wilcoxon (W)/Kruskal–Wallis (KW) tests by estimating P values through exact test or Monte Carlo approach.
- Two-way ANOVA was fitted in the presence of design involving more than one factor and in case of an interaction effect, the main effect was single investigated.
- Friedman two-way nonparametric ANOVA was fitted to jointly consider observations obtained from experiments performed at different times.
- Spearman rank correlation coefficient (rs) and its 95% confidence interval (CI) were used to quantify the strength of association between two continuous variables.
- Mixed model (with a compound symmetry covariance matrix) was fitted to assess the tumor growth as a function of time and experimental group (fixed factors) with mice considered as random factor. The same approach was used to compare the percentage of $CD11b^+$ cells in the PB during different time points.

Graph analyses were performed using GraphPad Prism Software (Version 9.0).

Public human dataset analysis was performed using R software. PB mononuclear cell raw data were downloaded from GSE27562 with the GEOquery package and then normalized with RMA function from affy package. Data were collapsed with the maxRowVariance method imported from WGCNA package. Class comparison between normal initial mammograms and patients with malignant breast cancer were performed through limma package and *P* value obtained from comparison was corrected with Benjamini–Hochberg method. Genes with a FDR < 0.05 were considered significant. *ATF3* variation between normal and malignant samples was charted through a boxplot for a graphical purpose.

Regarding the analysis of human expression data collected at Fondazione IRCCS Istituto Nazionale dei Tumori di Milano (18):

- The association between the tumors diagnosis (malignant vs. benign tumors) and the *ATF3* gene expression, normalized to *RPLP1* gene, was assessed by resorting to the nonparametric Kruskal–Wallis test.
- Differences in percentage of immune cells populations between groups of interest (malignant vs. benign tumors) were evaluated by applying a *t* test.
- Spearman rank correlation coefficient and its 95% CI were used to quantify the correlation between the percentage of $CD11b^+$ cells and *ATF3* expression levels.

The predictive capability of $CD11b^+$ cells was calculated as the area under the receiver operating characteristic ROC curve (AUC) and its corresponding 95% CI generated by resorting to a logistic regression model.

All the above analyses were performed using SAS software (Version 9.4.; SAS Institute, Inc.) by considering a significance level of alpha = 0.05.

Data availability

Expression data derived from mouse MSCs were deposited in the NCBI Gene Expression Omnibus database with the accession number GSE194032.

Results

The nuclear translocation of ATF3 in myeloid progenitor clusters is an early event of cancer-adapted hematopoiesis

GEPs of normal human and mouse hematopoiesis show *ATF3* expression almost restricted to monocytes (Supplementary Fig. S1A and S1B). IHC analysis of BM sections from transgenic BALB-NeuT (NeuT hereafter) shows increased ATF3 expression in NeuT compared with nontransgenic sibling BALB/c female mice, suggesting a role for ATF3 in cancer-adapted hematopoiesis (Supplementary Fig. S1C). To gain information on which BM cell upregulate ATF3, megakaryocyte/erythroid progenitors (MEP), CMPs, GMPs and mature cells (granulocytes and monocytes) were sorted (Supplementary Fig. S1D for the gating strategy) from the BM NeuT and control mice of 12 and 24 weeks of age, representative of early and late stages of breast cancer tumorigenesis, respectively (10, 19). qPCR analysis showed increased expression of *Atf3* in myeloid progenitors (CMPs, $CD34^+CD16/32$-, and GMP, $CD34^+CD16/32^+$) at early but not late stage of disease (**Fig. 1A–D**). On the contrary, *ATF3* was upregulated in monocytes ($Ly6C^{high}$) at late but not early stage of transformation (**Fig. 1A–D**; Supplementary Fig. S1D for gating strategy). The increased early expression of *Atf3* in CMPs was confirmed in the 41c transplantable model of breast cancer (originally derived from transgenic PyMT mice; ref. 15) in which the BM was analyzed when tumors were barely palpable (9 days post injection: Supplementary Fig. S1E).

As the translocation of ATF3 into the nucleus is a hallmark of its functional activation, we evaluated ATF3 by confocal microscopy on BM sections. **Figure 1E** and the relative quantifications (**Fig. 1F** and **G**) shows an increased nuclear translocation of ATF3 in NeuT in

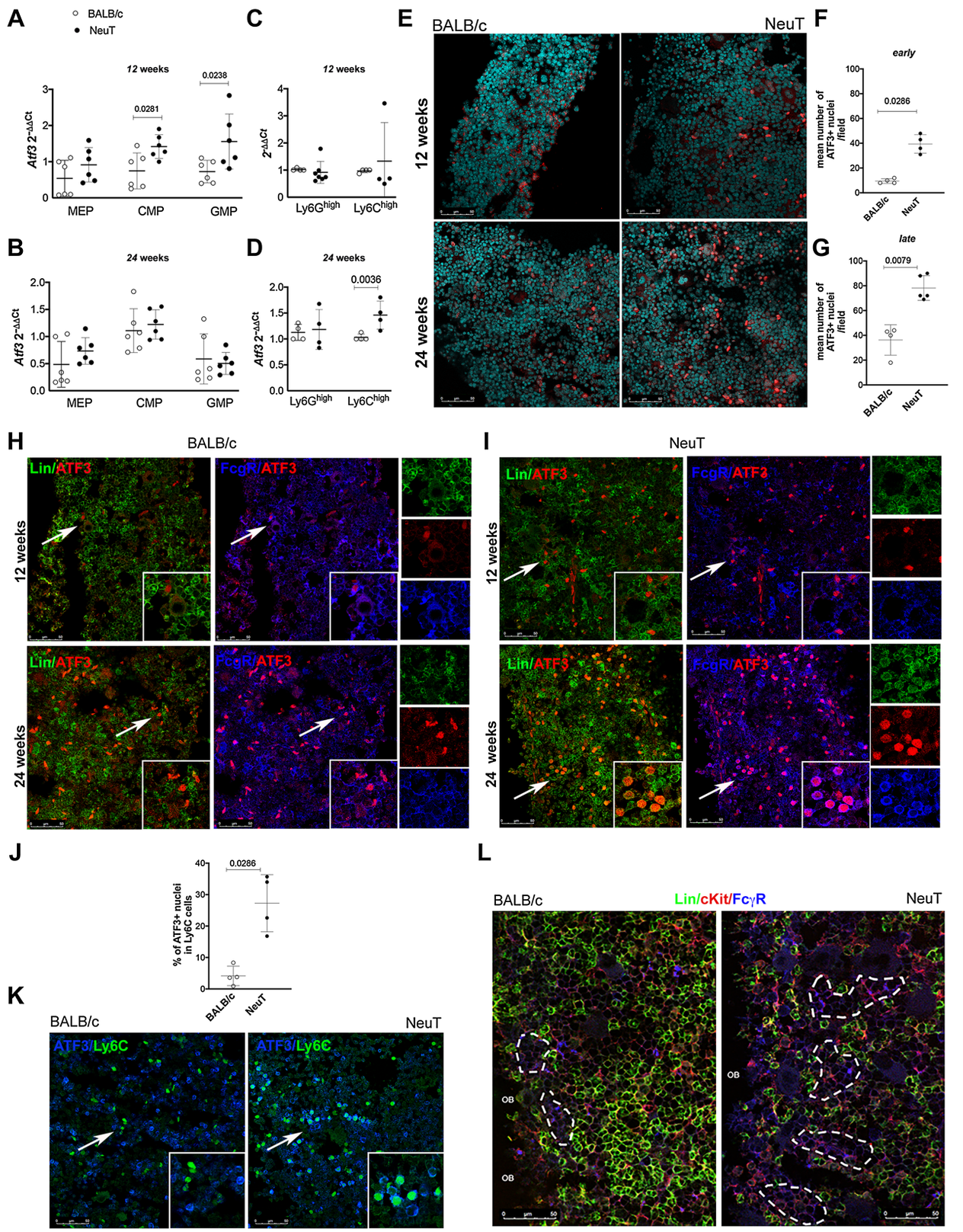
A
BALB/c
NeuT
12 weeks
0.0281
0.0238
Atf3 2−ΔΔCt
MEP
CMP
GMP
B
24 weeks
C
12 weeks
2−ΔΔCt
Ly6Ghigh
Ly6Chigh
D
24 weeks
0.0036
E
BALB/c
NeuT
12 weeks
24 weeks
F
early
0.0286
mean number of ATF3+ nuclei /field
G
late
0.0079
H
BALB/c
Lin/ATF3
FcgR/ATF3
I
NeuT
J
0.0286
% of ATF3+ nuclei in Ly6C cells
K
ATF3/Ly6C
L
Lin/cKit/FcγR
OB

comparison to controls at both early and late stages of disease. To identify which cell had ATF3 translocated into the nucleus, we performed a triple immunofluorescence for ATF3 (red), FcγR, (blue) and lineage (Lin) markers (green) on the same BM samples (**Fig. 1H** and **I**). In NeuT mice of 12 weeks of age, the analysis showed nuclear localization of ATF3 in cells negative for lineage markers (Lin) but positive for FcγR, suggesting their belonging to myeloid precursors (**Fig. 1I**). At this time point, the nontransgenic, tumor free, BALB/c siblings have limited ATF3 nuclear translocation in the same cell subset, suggesting that this event is stimulated by the peripheral transformation (**Fig. 1H** and **I**). At 24 weeks, both NeuT and siblings controls show increased nuclear localization of ATF3 although in different compartments, which are the mature myeloid cells ($Lin^+/Fc\gamma R^+$) in NeuT mice (**Fig. 1H** and **I**) and the $Lin^-/Fc\gamma R^+$ precursors in siblings controls (**Fig. 1H** and **I**). Furthermore, immunofluorescence analysis for ATF3 and Ly6C identified $Ly6C^+$ monocytes as the cell subset mostly enriched for ATF3 nuclear translocation in NeuT but not in sibling controls (**Fig. 1J** and **K**).

Notably, at early time point of tumorigenesis, the activation of ATF3 in myeloid progenitors was paralleled by the formation of GMP/CMP clusters (Lin^-/c-$Kit^+/Fc\gamma R^+$), identified by confocal microscopy analysis. Differently from nontransgenic siblings, which show GMPs/CMPs organized in small clusters, mainly located close to the osteoblastic niche (**Fig. 1L**), the GMPs/CMPs clusters of NeuT mice were larger, composed by higher number of cells and localized in the whole BM parenchyma (**Fig. 1L**), a clear feature of the emergency hematopoiesis.

Finally, to assess whether ATF3 expression and nuclear translocation in BM myeloid progenitors was a feature of cancer-related myelopoiesis or a more general mechanism induced by stress conditions (20), we analyzed ATF3 activation in the BM of mice chronically treated with LPS. In this setting, we observed ATF3 nuclear translocation that, differently from tumor-bearing mice, was confined to stromal cells localized nearby the osteoblastic niche, without involving myeloid progenitors (Supplementary Fig. S2A). In line, no changes were observed in the fraction of HSC precursors, as evaluated by FACS (Supplementary Fig. S2B).

Collectively, these findings indicate that the induction of ATF3 expression and its nuclear translocation in immature myeloid cells (CMP/GMP) and $Ly6C^+$ myeloid cells are specific feature of tumor-induced myelopoiesis. The distinct temporal activation of ATF3 in precursors versus $Ly6C^+$ myeloid cells might suggest a different role of ATF3 at early and late stages of disease, possibly involved in progenitor cell expansion and monocytes differentiation, respectively.

BM mesenchymal stroma cells sense peripheral tumor and in turn activate the NLRP3 inflammasome pathways and the release of IL1B

Stroma-derived BM niche signals have been largely involved in driving emergency hematopoiesis (21, 22). To evaluate whether the release of soluble mediators from MSCs was responsible for *Atf3* induction in progenitor cells, naïve HSCs were cocultured, using a transwell assay, with MSCs isolated from the bone of either NeuT or nontransgenic siblings mice. qPCR analysis shows that the expression of *Atf3* was upregulated in HSCs cocultured with MSCs isolated from NeuT mice (**Fig. 2A**; Supplementary Fig. S3A for purity check). To identify the upstream regulator of *Atf3*, we applied the IPA to a GEP performed on the BM of NeuT mice (GSE117071), by which we initially identified *Atf3* among the top up-modulated genes at the preinvasive stage of disease (10). Among the upstream regulator of *Atf3* results indicated IL1B (**Fig. 2B**), a proinflammatory cytokine able to stimulate HSCs proliferation, GMP clustering and myeloid differentiation (8). Considering that the above-mentioned dataset accounts for total BM cells, we performed a GEP analysis restricted to BM-MSCs collected at 12 and 24 weeks from the bone of NeuT mice and sibling BALB/c controls, for comparison. BM-MSCs were purified from the femurs and tibias of mice by immunomagnetic beads and phenotypically characterized by flow cytometry prior transcriptome analysis ($CD45^-$, $Ter119^-$, $CD31^-$, $CD29^+$; $CD44^+$; Supplementary Fig. S3B and S3C).

GEP analysis identified 367 genes significantly up-modulated (FDR ≤ 0.05) and 71 genes down-modulated (FDR ≤ 0.05) at early time points (**Fig. 2C**), whereas 17 genes were up- and 7 genes down-modulated at late time points (**Fig. 2C**) compared with age-matched BALB/c mice. *Nlrp3* and *Nlrp1b*, two well-known inflammasome gene member of the nod-like receptor (NLR) family, were commonly upregulated in BM-MSCs from NeuT mice at early and late time points, compared with controls (Supplementary Table S1A and S1B). GO indicated *Il1* and *Il1b* expression significantly enriched in BM-MSCs isolated from NeuT mice (**Fig. 2D** and **E**). Although NLR gene family was upregulated in the MSCs of NeuT mice collected at both early and late time points, some key genes belonging to the NLR inflammasome activation, including *Nlrp3,* and *Il1b* were significantly upregulated only in MSCs isolated from NeuT mice at early time points (**Fig. 2F** and **G**). The upregulation of *Il1b* and of *Nlrp3* expression in early MSCs was validated also through qPCR analysis performed on 12 weeks BM-MSCs (**Fig. 2H** and **I**) and in another cohort of *ex vivo* isolated BM-MSCs in which we compared early and late time points for *Il1b* expression (**Fig. 2J**).

To check whether soluble factors were responsible for the induction of *Il1b* in BM-MSCs, naïve MSCs were treated with the sera

Figure 1.

ATF3 expression and nuclear translocation is a hallmark of tumor-promoted myelopoiesis. **A–D,** Evaluation of *Atf3* expression by qPCR in FACS-sorted cells isolated from the BM of BALB/c and NeuT mice at early and late points: BM precursors at 12 weeks (P test; MEP, *P* value: 0.2121; CMP, *P* value: 0.0281; GMP, *P* value: 0.0238; **A**) and at 24 weeks of disease (P test; MEP, *P* value: 0.2338; CMP, *P* value: 0.5866; GMP, *P* value: 0.7143; **B**); mature $Ly6G^{high}$ and $Ly6C^{high}$ cells at 12 weeks of age (Friedman test; $Ly6G^{high}$, *P* value: 0.641; $Ly6C^{high}$, *P* value: 0.3004; **C**) and at 24 weeks of age (Friedman test; $Ly6G^{high}$, *P* value: 0.6298; $Ly6C^{high}$, *P* value: 0.0036; **D**). **E–G,** Confocal microscopy analysis showing overall ATF3 nuclear translocation in BM sections from NeuT and BALB/c mice at 12 and 24 weeks of age. **E,** Representative immunofluorescence analysis. ATF3, red; DAPI, cyan. **F** and **G,** Quantification of ATF3 nuclear localization at early and late time points (early, P test, *P* value: 0.0286; late, *P* value: 0.0079). Data are expressed as frequency of $ATF3^+$ nuclei/total nuclei. **H** and **I,** Confocal microscopy analysis for Lin (green), ATF3 (red), and FcγR (blue) performed at 12 and 24 weeks of age in BALB/c and NeuT mice. Arrows, enlarged area. The representative images show at 12 weeks of age, ATF3 nuclear signal was mainly localized in $Lin^-Fc\gamma R^+$ cells but not in $Lin^+ Fc\gamma R^+$ myeloid populations in both BALB/c and NeuT mice, with the difference that in BALB/c mice, ATF3 staining was only barely detectable. At late time points, ATF3 nuclear localization increased in both BALB/c mice and NeuT mice, where it characterized BM progenitors (Lin^-c-Kit^+) or mature ($Lin^+Fc\gamma R^+$) myeloid cells, respectively. **J** and **K,** Confocal microscopy analysis for ATF3 (green) and Ly6C (blue) in BM sections from BALB/c and NeuT mice at late time points (24 weeks). **J,** Quantification of ATF3 nuclear localization in $Ly6C^+$ cells (P test, *P* value: 0.0286). **K,** Representative images showing ATF3 confined in a portion of $Ly6C^+$ cells only in NeuT and not age-matched controls. **L,** Imaging of CMP/GMP clustering performed on frozen BM OCT samples from naïve (left) and tumor-bearing NeuT mice (right) at 12 weeks. Lin, green; c-Kit, red; FcγR, blue. Dotted lines, CMP/GMP clusters.

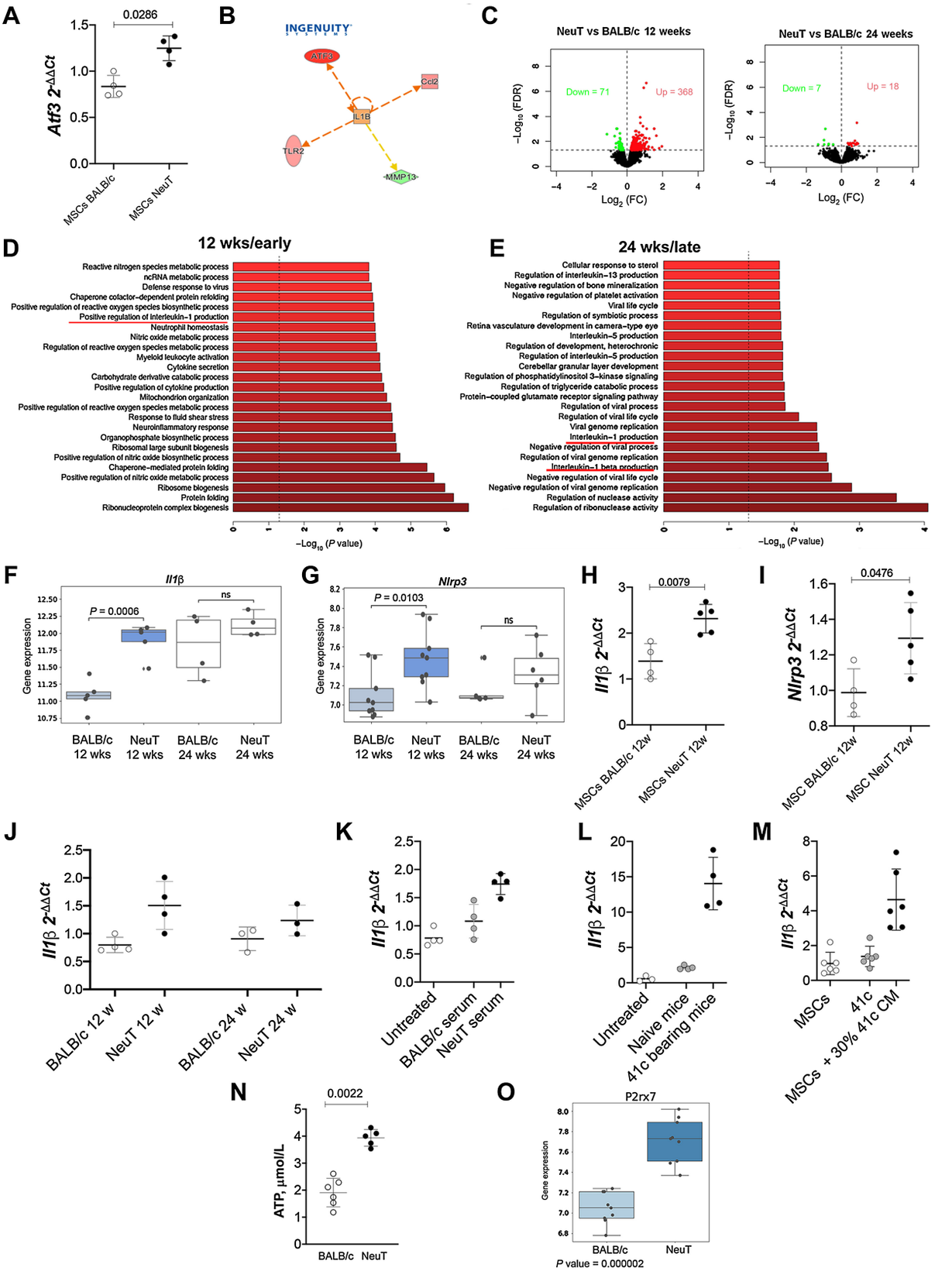
A
0.0286
Atf3 2-ΔΔCt
MSCs BALB/c
MSCs NeuT
B
INGENUITY SYSTEMS
ATF3
Ccl2
IL1B
TLR2
MMP13
C
NeuT vs BALB/c 12 weeks
Down = 71
Up = 368
NeuT vs BALB/c 24 weeks
Down = 7
Up = 18
−Log10 (FDR)
Log2 (FC)
D
12 wks/early
Reactive nitrogen species metabolic process
ncRNA metabolic process
Defense response to virus
Chaperone cofactor-dependent protein refolding
Positive regulation of reactive oxygen species biosynthetic process
Positive regulation of interleukin-1 production
Neutrophil homeostasis
Nitric oxide metabolic process
Regulation of reactive oxygen species metabolic process
Myeloid leukocyte activation
Cytokine secretion
Carbohydrate derivative catabolic process
Positive regulation of cytokine production
Mitochondrion organization
Positive regulation of reactive oxygen species metabolic process
Response to fluid shear stress
Neuroinflammatory response
Organophosphate biosynthetic process
Ribosomal large subunit biogenesis
Positive regulation of nitric oxide biosynthetic process
Chaperone-mediated protein folding
Positive regulation of nitric oxide metabolic process
Ribosome biogenesis
Protein folding
Ribonucleoprotein complex biogenesis
−Log10 (P value)
E
24 wks/late
Cellular response to sterol
Regulation of interleukin-13 production
Negative regulation of bone mineralization
Negative regulation of platelet activation
Viral life cycle
Regulation of symbiotic process
Retina vasculature development in camera-type eye
Interleukin-5 production
Regulation of development, heterochronic
Regulation of interleukin-5 production
Cerebellar granular layer development
Regulation of phosphatidylinositol 3-kinase signaling
Regulation of triglyceride catabolic process
Protein-coupled glutamate receptor signaling pathway
Regulation of viral process
Regulation of viral life cycle
Viral genome replication
Interleukin-1 production
Negative regulation of viral process
Regulation of viral genome replication
Interleukin-1 beta production
Negative regulation of viral life cycle
Negative regulation of viral genome replication
Regulation of nuclease activity
Regulation of ribonuclease activity
−Log10 (P value)
F
Il1β
P = 0.0006
ns
Gene expression
BALB/c 12 wks
NeuT 12 wks
BALB/c 24 wks
NeuT 24 wks
G
Nlrp3
P = 0.0103
ns
Gene expression
BALB/c 12 wks
NeuT 12 wks
BALB/c 24 wks
NeuT 24 wks
H
0.0079
Il1β 2-ΔΔCt
MSCs BALB/c 12w
MSCs NeuT 12w
I
0.0476
Nlrp3 2-ΔΔCt
MSC BALB/c 12w
MSC NeuT 12w
J
Il1β 2-ΔΔCt
BALB/c 12 w
NeuT 12 w
BALB/c 24 w
NeuT 24 w
K
Il1β 2-ΔΔCt
Untreated
BALB/c serum
NeuT serum
L
Il1β 2-ΔΔCt
Untreated
Naive mice
41c bearing mice
M
Il1β 2-ΔΔCt
MSCs
41c
MSCs + 30% 41c CM
N
0.0022
ATP, µmol/L
BALB/c
NeuT
O
P2rx7
Gene expression
BALB/c
NeuT
P value = 0.000002

collected from NeuT mice of 12 weeks of age or controls. **Figure 2K** shows that the treatment with the serum from NeuT mice significantly induced *Il1b* expression in BM-MSCs. Notably, a similar induction occurred when BM-MSCs were exposed to either serum collected from mice bearing 41c mammary tumors (**Fig. 2L**) or 41c-conditioned medium (**Fig. 2M**). The last experiment also show that 41c cells per se do not express *Il1b*, indicating circulating or tumor-released factors as responsible for the induction of *Il1b* in BM-MSCs. As the known main upstream regulator of the NLRP3/inflammasome is extracellular ATP (eATP; ref. 23), we quantified this mediator in plasma collected from NeuT and sibling controls. Significant increase of eATP serum level was found in in NeuT than control mice (**Fig. 2N**), a data that fits well with the increased expression of the cognate receptor P2rx7 in BM-MSCs of NeuT than control mice (**Fig. 2O**).

IL1B signaling drives ATF3 activation in HSCs and initiates a specific lineage commitment

The activation of the NLRP3 inflammasome signaling pathway and the expression of *Il1b* in BM-MSCs of NeuT mice prompted us to verify whether it is directly responsible for ATF3 upregulation and nuclear translocation in HSCs. To assess IL1B effect on ATF3 activation, HSCs cells were stimulated with recombinant IL1B also in the presence of mAb blocking IL1B or the isotype control. Confocal microscopy analysis shows that the presence of IL1B blocking mAb, but not of the isotype control, inhibited IL1B nuclear translocation (**Fig. 3A**).

To confirm that the activation of ATF3 is specifically mediated by the release of IL1B from NeuT-derived BM-MSCs, we performed coculture between HSCs and BM-MSCs in presence of an anti-IL1B mAb or isotype control. qPCR analysis showed a reduced *Atf3* expression in presence of the IL1B blocking mAb (**Fig. 3B**).

To assess the relevance of this pathway *in vivo*, NeuT mice were treated with the IL1B blocking mAb, twice a week, starting at 12 weeks of age, for a total of 4 weeks. At sacrifice, the BMs were collected to estimate *Atf3* expression in HSC populations. The treatment induced *Atf3* down-modulation in HSCs (**Fig. 3C**) along with a substantial decrease of GMPs as evaluated by FACS (**Fig. 3D**). Notably, the *in vitro* treatment reduced the nuclear translocation of ATF3 (**Fig. 3E** and **F**) along with the reduction in the clustering of CMP/GMP (**Fig. 3G**), both evaluated by confocal microscopy on BM sections.

To gain further insights and corroborate these data, we used the transplantable 41c model. Mature and immature populations from the BM of 41c-injected mice, treated or not with anti-IL1B mAb, were sorted and *Atf3* expression was evaluated by qPCR. The treatment with anti-IL1B Ab significantly reduced *Atf3* expression in all immature (HSCs, MEPs, CMPs and GMPs) and mature (Ly6G and Ly6C) myeloid cells (**Fig. 3H**), also reducing the frequency of GMP and CD11b in the BM of treated mice (**Fig. 3I** and **J**). Overall, these findings suggest that *Atf3* induction in HSCs could be a necessary step toward myeloid differentiation.

ATF3 deletion in the myeloid compartment affects the monocyte frequency and their differentiation into macrophages

Besides being activated in myeloid precursors at early time point, ATF3 became activated in mature myeloid cells, particularly in monocytes, at later stage of cancer progression (**Fig. 1**). This suggests that early ATF3 activation in CMPs/GMPs might drive their further differentiation toward cells of monocytic lineage. To assess the relevance of ATF3 in monocyte differentiation, we evaluated *Atf3* expression in Lin- cells treated for 9 days with M-CSF. As shown by qPCR, *Atf3* expression increased during differentiation of Lin^- cells toward monocytes/macrophages (**Fig. 4A**). Notably, this phenotype correlated with the induction of *Irf8* (r_s: 0.91; 95% CI, 0.75–0.97), a transcription factor involved in monocyte differentiation (**Fig. 4B**; refs. 24, 25), along with the gaining of the F4/80 macrophage-specific surface marker (r_s: 0.79; 95% CI, 0.47–0.92; **Fig. 4C**).

To verify, through a different approach, whether ATF3 in Lin- cells skews progenitor differentiation toward monocytes, Lin- cells were infected with a lentiviral vector designed to force *Atf3* expression under the myeloid-specific CD68 promoter, which is expressed in progenitors starting from the CMP/GMP stage and in differentiated myeloid cells (DC, monocytes and, at low levels, in granulocytes; refs. 26–28). Results showed that *Atf3* overexpression promotes the expansion and differentiation of monocyte/macrophage colony forming units (Supplementary Fig. S4).

Finally, to test whether the deletion of *Atf3* in the myeloid compartment was able to affect tumor progression, the 41c cell line was injected into the mammary fat pad of $Atf3^{fl/fl}$LysMCre$^{+/-}$ and $Atf3^{fl/fl}$LysMCre$^{-/-}$ control mice. The efficiency and specificity of Cre expression in $Atf3^{fl/fl}$LysMCre$^{+/-}$ mice was evaluated on sorted BM myeloid cell populations and peritoneal macrophages isolated *ex vivo*, checking *Atf3* expression by qPCR. The expression of *Atf3* decreased in all mature myeloid populations in $Atf3^{fl/fl}$LysMCre$^{+/-}$ compared with controls (Supplementary Fig. S5A). Thirty days after tumor injection, mice were sacrificed and tumor and PB were analyzed to detect possible differences in immune cell composition. Flow cytometry analyses revealed a decrease in monocytes (Ly6C^{high}) in PB (**Fig. 4D**) and tumors (**Fig. 4E**) of $Atf3^{fl/fl}$LysMCre$^{+/-}$ mice in comparison to $Atf3^{fl/fl}$ controls.

Having shown that ATF3 plays a role in monocyte to macrophage differentiation, we evaluated the presence of macrophages in situ in tumors obtained from $Atf3^{fl/fl}$LysMCre$^{+/-}$ and $Atf3^{fl/fl}$ mice. IHC

Figure 2.

MSCs sense peripheral tumor, activate the NLRP3 inflammasome signaling pathway, and release Il1b. **A,** qPCR for *Atf3* expression in HSCs cocultured with BALB/c or NeuT-derived BM-MSCs (P test, *P* value: 0.0286). **B,** Output of IPA software analysis showing the putative relation between IL1B and ATF3. Red and green indicate whether the genes are upregulated or downregulated, respectively. Dashed line, indirect interaction. **C,** Volcano plots obtained from the comparison of GEPs of NeuT and BALB/c BM-derived MSCs samples at 12 and 24 weeks of age. Red and green points show significantly up- or down-modulated genes, respectively (FDR < 0.05 and absolute FC 1). **D** and **E,** Barplot showing the top 25 GO terms significantly enriched in the list of genes upregulated at 12 and 24 weeks of age between BM-MSCs isolated from NeuT versus BALB/c mice. **F** and **G,** Bar plots showing the expression of *Il1b* and *Nlrp3* genes in the GEP at both time points. **H** and **I,** qPCR for *Nlrp3* and *Il1b* genes evaluated on purified BM-MSCs isolated from BALB/c and NeuT at early time point (12 weeks; P test, *Il1b*, *P* value: 0.0079; *Nlrp3*, *P* value: 0.0476). **J,** Validation by qPCR of *Il1b* upregulation in a new cohort of MSCs isolated from NeuT and control sibling mice at 12 and 24 weeks of age (ANOVA 2-way test, *P* value mice: 0.0057; *P* value time: 0.6320). **K,** Evaluation of *Il1b* by qPCR after stimulation of BALB/c-derived BM-MSCs with serum collected from tumor-free (BALB/c) and -bearing (NeuT) mice (KW test, *P* value: 0.0008). **L,** Evaluation of *Il1b* by qPCR after stimulation of BALB/c-derived BM-MSCs with serum collected from tumor-free (C57) and mice bearing 41c tumors (KW test, *P* value: 0.0001). **M,** Evaluation of *Il1b* by qPCR in BM-MSCs alone, 41c alone, and BM-MSCs after stimulation with 41c conditioned medium (KW test, *P* value: < 0.0001). **N,** ATP level in plasma collected from NeuT and BALB/c controls (P test, *P* value: 0.0022). **O,** *P2rx7* expression level in the GEP of BALB/c and NeuT BM-MSCs.

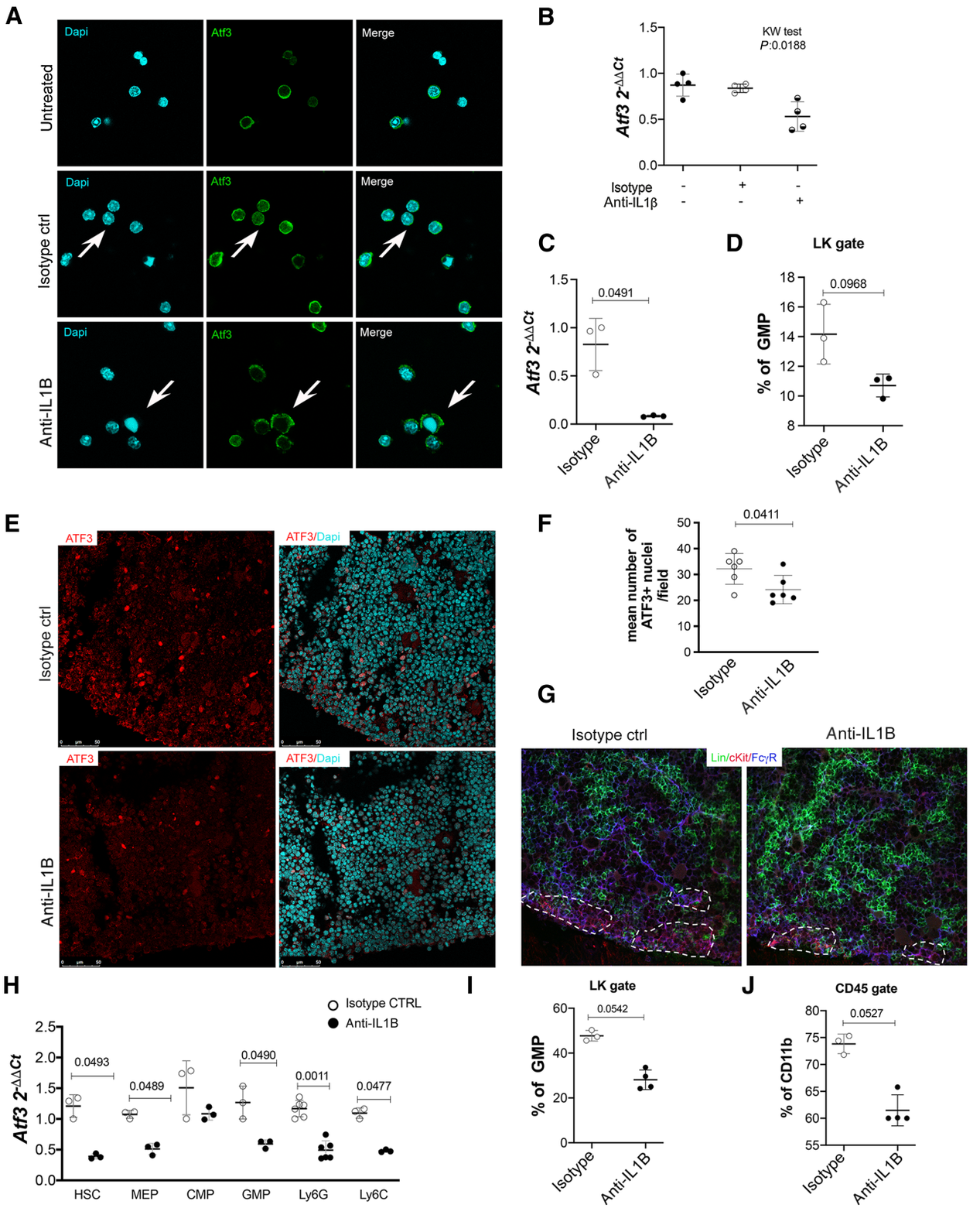
A
Dapi
Atf3
Merge
Untreated
Isotype ctrl
Anti-IL1B
B
KW test
P:0.0188
Atf3 2-ΔΔCt
Isotype
Anti-IL1β
C
0.0491
Atf3 2-ΔΔCt
Isotype
Anti-IL1B
D
LK gate
0.0968
% of GMP
E
ATF3
ATF3/Dapi
F
0.0411
mean number of ATF3+ nuclei /field
G
Isotype ctrl
Anti-IL1B
Lin/cKit/FcγR
H
Isotype CTRL
Anti-IL1B
0.0493
0.0489
0.0490
0.0011
0.0477
HSC
MEP
CMP
GMP
Ly6G
Ly6C
I
LK gate
0.0542
% of GMP
J
CD45 gate
0.0527
% of CD11b

analysis showed a reduction of CD206+ macrophages in tumors from *Atf3*$^{fl/fl}$LysMCre$^{+/-}$ (**Fig. 4F** and **G**). In these same tumors, hematoxylin and eosin (H&E) analysis showed abnormal deposition of fibrotic nuclear material, a picture compatible with the absence of scavenger tumor-associated macrophages (TAM; Supplementary Fig. S5B). These findings are compatible with an overall decrease of local macrophage differentiation, which is also in line with the reduced number of circulating monocytes observed in conditional *Atf3* knockout mice. Furthermore H&E showed larger hypoxic and necrotic areas, more evident infiltrative growth with better integration with the surrounding tumor stroma and increased lymphocytes in tumors from *Atf3*$^{fl/fl}$LysMCre$^{+/-}$ than from *Atf3*$^{fl/fl}$ controls (Supplementary Fig. S5B). The increased lymphocytes infiltration found in H&E sections was confirmed by IHC analysis showing higher CD8+ T cells in tumors obtained from *Atf3*$^{fl/fl}$LysMCre$^{+/-}$ than control mice (**Fig. 4F–H**).

To test the CD8 T cells involvement, *Atf3*$^{fl/fl}$LysMCre$^{+/-}$ and controls were injected with the PyMT-derived 41c cell line harnessed to express a model antigen (human mutated nucleophosmin; ref. 16) and treated or not with α-PD1. Data show an increased efficacy of α-PD1 in *Atf3*$^{fl/fl}$LysMCre$^{+/-}$ than controls (**Fig. 4I**) paralleled by an increased frequency of proliferating CD8$^+$Ki67$^+$PD1$^+$TNF$^+$ cells (**Fig. 4J**).

ATF3 and CD11b$^+$ cells in the PB discriminate benign from malignant breast lesions

Having shown that ATF3 is a relevant functional marker of cancer-adapted myelopoiesis, we tested whether ATF3 could be exploited as a circulating marker of transformation. Hence, we tested its expression in the PB of NeuT mice collected at late stages of breast carcinogenesis (24 weeks), when myeloid cells are significantly released into the circulation (**Fig. 5A**). qPCR analysis showed that *Atf3* expression was higher in the PB of NeuT compared with age-matched control BALB/c mice (**Fig. 5B**). To investigate the translational significance of these data, we evaluated *ATF3* expression *in silico* in a public dataset (GSE27562) consisting of PBMC collected from 57 patients with a diagnosis of breast cancer versus 31 healthy controls (29). Data confirmed *ATF3* upregulation in PBMCs from BC patients compared with controls [Fold change (FC) = 1.7, FDR = 0.002; **Fig. 5C**].

Next, we tested whether *ATF3* was also able to discriminate among patients with benign or malignant mammary lesions, with uncertainty diagnostic radiology. To this end, we analyzed the PBMCs of 43 patients with a suspected breast cancer enrolled in our institute in the Breast Blood Early diagnosis (BABE) study (18). qPCR analysis of *ATF3* expression in the CD14$^+$ monocytic fraction along with a multiparametric flow cytometry analysis testing myeloid cell composition, were performed on PBMCs collected from patients prior to tissue biopsies, which then identified 24 benign versus 19 malignant breast lesions (Supplementary Table S2). Notably, the percentage of CD11b$^+$ cells, evaluated by flow cytometry analysis, was able to discriminate benign from malignant patients (**Fig. 5D**) as occurring in the mouse model. Although *ATF3* level detected by qPCR analysis was not able, per se, to discriminate among the 2 groups (**Fig. 5E**), we found a positive correlation between *ATF3* and the percentage of CD11b$^+$ cells only in patients with malignant conditions (r_s, 0.57; 95% CI, 0.14–0.81), whereas a negative correlation was found in patients with a benign diagnosis (r_s, −0.54; 95% CI, −0.77 to −0.16; **Fig. 5F** and **G**). To deeper investigate the role of ATF3 combined to CD11b$^+$ in discriminating benign and malignant condition, a logistic regression model was implemented including the two markers and their interaction, the predictive capability of CD11b$^+$ quantified through the AUC was improved (**Fig. 5H**). This data suggests that a combined evaluation of CD11b$^+$ cells and *ATF3* expression in the PB CD14$^+$ cells could be used, in association with other markers i.e., circulating miRNAs (18), to discriminate among women with benign versus malignant transformation, avoiding unnecessary invasive procedure.

Discussion

The response of the BM to chronic stress conditions, including cancer, has been largely considered in terms of myeloid cell efflux from BM to circulation. Here we provide some evidences indicating that first sensors of incipient breast tumors are the BM-MSC that, through the production of IL1B, promote ATF3 expression and nuclear translocation in HSCs. The activation of ATF3 is a necessary step to support all features of cancer-adapted myelopoiesis from HSC differentiation into myeloid cell precursors to cell fate decision (monocytes and TAM. Graphical abstract). Furthermore, data obtained analyzing the PB of patients with breast cancer candidate the presence of circulating *ATF3*-expressing monocytes as possible marker able to discriminate between benign and malignant cases.

The activation of another member of the ATF/CREB family of transcription factors, namely ATF6, has been recently involved in driving polymorphonuclear myeloid-derived suppressor cell activity in lung cancer (30). These data fit well with the concept that although all tumors can increase the hematopoietic demand, the expansion of specific subpopulations could be "qualitatively" different according to the tumor tissue of origin and their signals to the BM for activation of specific lineage-determining transcription factors.

We describe the BM response to nascent breast tumor involving the sequential upregulation and nuclear translocation of ATF3 in two different subsets of BM cells. At early time points, corresponding to incipient tumors, the nuclear translocation of ATF3 in BM progenitor cells promotes the formation of CMP/GMP clusters, which

Figure 3.
IL1B drives ATF3 activation in HSCs and initiates a specific lineage commitment. **A,** Confocal microscopy for ATF3 (green) on naïve HSCs stimulated *in vitro* with recombinant IL1B ± anti-IL1B showing ATF3 mainly localized in the nuclei of IL1B-stimulated HSCs (arrows) in presence of the Isotype control. In HSCs treated with the IL1B blocking mAB, ATF3 was localized mainly in the cytoplasm (arrows). **B,** *Atf3* expression on naïve HSCs cocultured with NeuT-derived BM-MSCs ± anti-IL1B or isotype CTRL (KW test, *P* value: 0.0188). **C,** *Atf3* expression by qPCR on HSCs sorted from the BM of NeuT mice, at premalignant stage of disease, treated or not with anti-IL1B antibody for 4 weeks. Each dot represents a pool of 3 to 4 mice (one-sided W test, *P* value: 0.0491). **D,** Percentage of GMPs within the Lin-c-Kit$^+$ cells evaluated by flow cytometry analysis on total BM cells collected from NeuT mice treated or not with anti-IL1B mAb (W test, *P* value: 0.0968). **E** and **F,** Confocal microscopy analysis for ATF3 in NeuT mice treated with mAb blocking Il1B or the isotype control. **E,** Representative image showing the decreased nuclear translocation of ATF3 in presence of mAb blocking IL1B. **F,** Relative quantification (P test, *P* value: 0.0411). **G,** Evaluation of CMP/GMP clustering on OCT-embedded BM sections. Lin, green; c-kit, red; FcyR, blue; DAPI, cyan. **H,** Evaluation of *Atf3* expression by qPCR on sorted progenitor and mature myeloid cells isolated from B6 mice injected with 41c tumor cell line and treated or not with aIL1B Ab. Each dot represents a pool of 3 to 4 mice (one-sided W test, HSC, *P* value: 0.0493; MEP, *P* value: 0.0489; CMP, *P* value: 0.1993; GMP, *P* value: 0.0490; Ly6C, *P* value: 0.0477; one-sided P test, Ly6G, *P* value: 0.0011). **I** and **J,** Percentage of GMPs and CD11b$^+$ cells evaluated by FACS analysis on BM cells collected from B6 mice injected with 41c tumor cell line ± anti-IL1B (W test, GMP, *P* value: 0.0542; CD11b, *P* value: 0.0527).

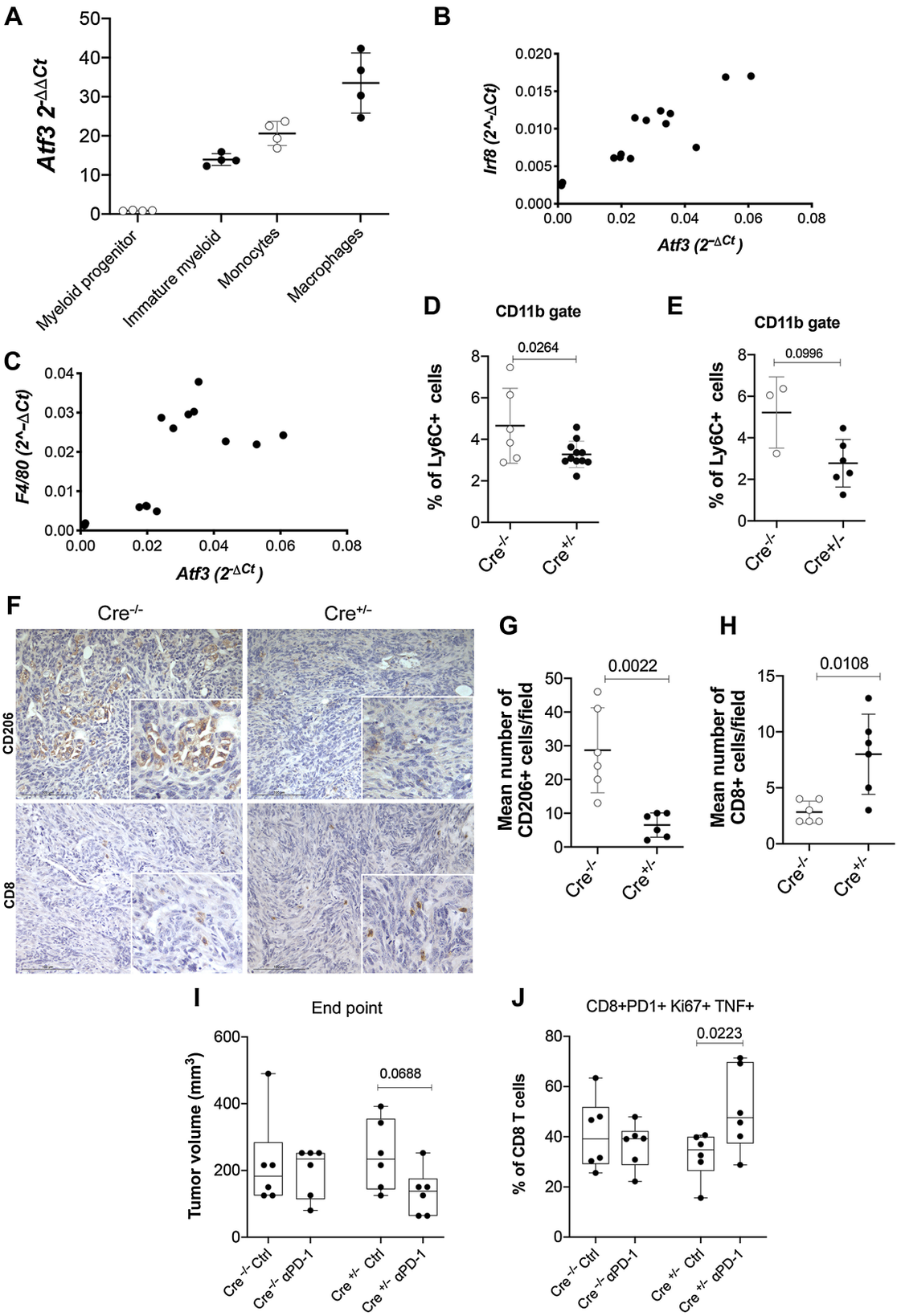
A
Atf3 2-ΔΔCt
50
40
30
20
10
0
Myeloid progenitor
Immature myeloid
Monocytes
Macrophages
B
Irf8 (2^-ΔCt)
0.020
0.015
0.010
0.005
0.000
0.00
0.02
0.04
0.06
0.08
Atf3 (2-ΔCt)
C
F4/80 (2^-ΔCt)
0.04
0.03
0.02
0.01
0.00
0.00
0.02
0.04
0.06
0.08
Atf3 (2-ΔCt)
D
CD11b gate
0.0264
% of Ly6C+ cells
8
6
4
2
0
Cre-/-
Cre+/-
E
CD11b gate
0.0996
% of Ly6C+ cells
8
6
4
2
0
Cre-/-
Cre+/-
F
Cre-/-
Cre+/-
CD206
CD8
G
0.0022
Mean number of CD206+ cells/field
50
40
30
20
10
0
Cre-/-
Cre+/-
H
0.0108
Mean number of CD8+ cells/field
15
10
5
0
Cre-/-
Cre+/-
I
End point
0.0688
Tumor volume (mm3)
600
400
200
0
Cre -/- Ctrl
Cre-/- αPD-1
Cre +/- Ctrl
Cre +/- αPD-1
J
CD8+PD1+ Ki67+ TNF+
0.0223
% of CD8 T cells
80
60
40
20
0
Cre -/- Ctrl
Cre-/- αPD-1
Cre +/- Ctrl
Cre +/- αPD-1

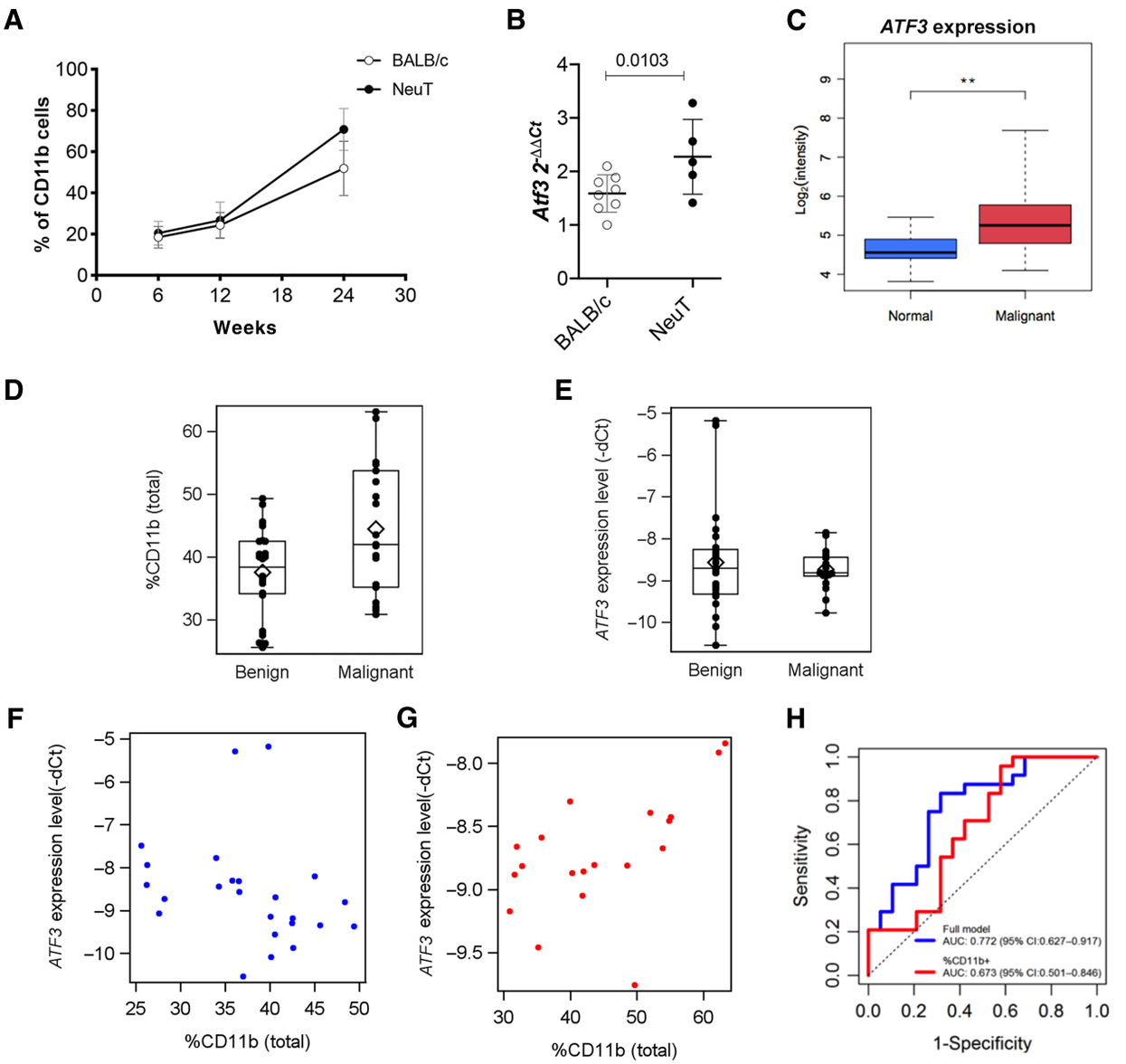

Figure 5.

ATF3^{+}CD14^{+} cells, in correlation with the expansion of CD11b^{+} population, discriminate benign vs. malignant transformation. **A,** Quantification of CD11b^{+} cells in the blood of BALB/c and NeuT mice starting from 6 weeks of age (mixed model, *P* value mice: 0.0221). **B,** *Atf3* expression evaluated by qPCR on total PBMCs isolated from the blood of BALB/c and NeuT mice (24 weeks). Dots, individual mice. (P test, *P* value: 0.0103). **C,** *ATF3* expression on PBMCs collected from healthy donors ($n = 31$) and patients with breast cancer ($n = 57$) based on GSE27562. **D,** Distribution of %CD11b (total) according to the type of tumor's diagnosis (*n* benign = 24 vs. *n* malignant = 19; *t* test on transformed values, *P* value: 0.0128). **E,** Distribution of *ATF3* gene as −dCt, according to the type of tumor's diagnosis (*n* benign = 24 vs. *n* malignant = 19; KW, *P* value: 0.9902). Each box indicates the 25th and 75th centiles. The horizontal line and the diamond inside the box indicate the median and the mean, respectively. The whiskers indicate the extreme measured values and each point the value for the corresponding patient. **F** and **G,** Scatter plot showing the correlation of *ATF3* gene as −dCt (*x*-axis) and %CD11b (total; *y*-axis) in benign vs. malignant conditions. Blue and red points represent patients with benign and malignant tumor, respectively. **H,** Predictive capability of *ATF3* combined with CD11b. ROC curve from percentage of CD11b (red line) and full model (blue line).

Figure 4.

ATF3 drives monocyte/macrophage cell differentiation. **A,** *Atf3* expression evaluated by qPCR during different stages of monocyte/macrophage cell differentiation induced by M-CSF. For *in vitro* experiments, four biological replicates were used (KW test, $P < 0.0001$). **B** and **C,** Spearman correlation analysis between the levels of *Atf3* and the expression of *Irf8* and *F4/80*, markers of macrophage maturation. **D** and **E,** Quantification of monocytes (Ly6C^{high}) in the PB (P test, *P* value: 0.0264; **D**) and in the tumor of ATF3$^{fl/fl}$ (Cre$^{-/-}$) and ATF3$^{fl/fl}$LySMCre$^{+/-}$ (Cre$^{+/-}$) mice after injection of 41c tumor cell line (W test, *P* value: 0.0996; **E**). **F,** IHC staining of CD206^{+} macrophages and CD8^{+} T cells in 41c tumor sections of Cre$^{+/-}$ and relative Cre$^{-/-}$ control mice injected with 41c cancer cell line. **G** and **H,** Relative quantification. **I,** Tumor volume (end point) in mice treated with Isotype control or aPD1 (ANOVA contrast, Cre$^{-/-}$ isotype ctrl versus Cre$^{+/-}$ isotype ctrl, *P* value: 0.6605; Cre$^{-/-}$ aPD1 versus Cre$^{+/-}$ ctrl, *P* value: 0.3998; Cre$^{+/-}$ aPD1 versus Cre$^{\pm}$ isotype ctrl, *P* value: 0.0688). **J,** Frequency of CD8^{+}PD1^{+}Ki67^{+}TNF^{+} cells in tumor from mice treated with aPD1 or isotype control. ANOVA contrast, Cre$^{-/-}$ isotype ctrl versus Cre$^{+/-}$ isotype ctrl, *P* value: 0.2700; Cre$^{-/-}$ aPD1 versus Cre$^{+/-}$ ctrl, *P* value: 0.5890; Cre$^{+/-}$ aPD1 versus Cre$^{+/-}$ isotype ctrl, *P* value: 0.0223.

represent key features of emergency hematopoiesis (7). At late time points of tumor progression, ATF3 activation drives the expansion of monocytic-myeloid cells that differentiate into macrophages in peripheral tissues. The involvement of ATF3 in monocyte/macrophage differentiation was supported by data showing that ATF3 expression increases during monocyte/macrophage cell differentiation and that its overexpression in BM progenitor cells enhances their ability to form monocyte/macrophage colonies in a semisolid medium. Mechanistically, the effect of ATF3 on monocyte/macrophage differentiation involve the induction of *Irf8*, a transcription factor that drives progenitor cell differentiation into macrophages (25, 31).

In vivo, when PyMT-derived 41c tumors were transplanted into $Atf3^{fl/fl}$LysMCre$^{+/-}$ we detected reduced infiltrating TAMs along with lower frequency of PB monocytes in comparison to $Atf3^{fl/fl}$ control mice. Unexpectedly, such differences did not affect tumor growth that was similar in the two strains. In line, Wolford and coll. reported similar tumor take and size upon subcutaneous injection of MVT-1 mammary cell line into $Atf3^{fl/fl}$LysMCre$^{+/-}$ and control mice, whereas they observed a substantial reduction of lung metastasis in the former group upon orthotopic injection (32). However, using the 41c cell line harnessed to express a model antigen (human mutate nucleophosmin, NPMc+ (16) to assure immunogenicity, we found an increased efficacy of aPD-1 treatment, evaluated as reduction of tumor volume, in $Atf3^{fl/fl}$LysMCre$^{+/-}$ than controls, suggesting that targeting ATF3 in myeloid cells could improve the efficacy of immune checkpoint treatment.

We identified the activation of NLRP3/inflammasome and the release of IL1B by BM-MSCs as responsible for the initial induction of ATF3 in HSCs and the consequent release of monocytes into the PB. Looking at tumor derived/circulating factors able to promote the activation of the NLRP3/inflammosome in BM-MSCs, we tested eATP, which is a known regulator of this pathway (23) and found its increase in the sera of NeuT mice than controls. Other factors might contribute to inflammasome activation. Our preliminary analysis of circulating miRNA show a significant down-modulation of those predicted to target the inflammasome-signaling pathway common to NeuT mice and patients with breast cancer that need to be validated.

In our beast cancer models, not only the upregulation of ATF3 expression in HSC was tumor-specific, being the chronic administration of LPS unable to induce ATF3 activation in myeloid cells, but the presence of *ATF3*-expressing monocytes seems to work as biomarker for presence of incipient tumor in women and might suggest the targeting of ATF3.

Nevertheless, like for other transcription factors, the targeting of ATF3, could be difficult to achieve pharmacologically. However, the inhibition of IL1B, its upstream regulator, could be very feasible according to the Canakinumab Anti-inflammatory Thrombosis Outcomes Study (CANTOS) that showed reduced incidence of lung cancer in patients with atherosclerosis treated with anti-IL1B monoclonal Ab (33). Benefits were demonstrated also in patients with breast cancer. Indeed, an IL1 signature has been identified in HER-2–negative breast cancers with poor prognosis and treatment with anti-IL1R antagonist, anakinra, reduced the expression of inflammatory genes in PB leukocytes while increased the expression of several natural killer and cytotoxic T-cell genes (34).

In summary, our findings identify ATF3 as a relevant transcription factor that, activated in HSCs by tumor-primed BM-MSCs, redirects BM hematopoiesis toward monocytic cell expansion and differentiation into TAMs.

Authors' Disclosures

No disclosures were reported.

Authors' Contributions

M. Perrone: Investigation, writing–original draft. **C. Chiodoni:** Methodology. **M. Lecchi:** Formal analysis, statistical analysis. **L. Botti:** Investigation. **B. Bassani:** Investigation. **A. Piva:** Formal analysis, bioinformatic analysis. **E. Jachetti:** Investigation. **M. Milani:** Formal analysis. **D. Lecis:** Methodology. **E. Tagliabue:** Enrolled patients. **P. Verderio:** Formal analysis, writing–review and editing. **S. Sangaletti:** Supervision, writing–original draft, writing–review and editing. **M.P. Colombo:** Conceptualization, supervision, writing–review and editing.

Acknowledgments

The authors thank Dr. Tiziana Ada Renzi and Ester Grande for administrative assistance. They thank the Platform of Integrated Biology for microarray experiments and the Animal Facility at Fondazione IRCCS Istituto Nazionale dei Tumori.

The research leading to these results received funding from AIRC under IG 2020 - ID.24363 project - PI Mario P. Colombo and from AIRC under IG 2018 - ID.22204 project - PI Sabina Sangaletti.

The publication costs of this article were defrayed in part by the payment of publication fees. Therefore, and solely to indicate this fact, this article is hereby marked "advertisement" in accordance with 18 USC section 1734.

Note

Supplementary data for this article are available at Cancer Research Online (http://cancerres.aacrjournals.org/).

Received February 24, 2022; revised September 13, 2022; accepted October 28, 2022; published first November 1, 2022.

References

1. Sangaletti S, Tripodo C, Chiodoni C, Guarnotta C, Cappetti B, Casalini P, et al. Neutrophil extracellular traps mediate transfer of cytoplasmic neutrophil antigens to myeloid dendritic cells toward ANCA induction and associated autoimmunity. Blood 2012;120:3007–18.
2. Tripodo C, Burocchi A, Piccaluga PP, Chiodoni C, Portararo P, Cappetti B, et al. Persistent immune stimulation exacerbates genetically driven myeloproliferative disorders via stromal remodeling. Cancer Res 2017;77:3685–99.
3. Casbon AJ, Reynaud D, Park C, Khuc E, Gan DD, Schepers K, et al. Invasive breast cancer reprograms early myeloid differentiation in the bone marrow to generate immunosuppressive neutrophils. Proc Natl Acad Sci USA 2015;112:E566–75.
4. Engblom C, Pfirschke C, Zilionis R, Da Silva Martins J, Bos SA, Courties G, et al. Osteoblasts remotely supply lung tumors with cancer-promoting SiglecF(high) neutrophils. Science 2017;358:eaal5081.
5. Melani C, Chiodoni C, Forni G, Colombo MP. Myeloid cell expansion elicited by the progression of spontaneous mammary carcinomas in c-erbB-2 transgenic BALB/c mice suppresses immune reactivity. Blood 2003;102:2138–45.
6. Peinado H, Aleckovic M, Lavotshkin S, Matei I, Costa-Silva B, Moreno-Bueno G, et al. Melanoma exosomes educate bone marrow progenitor cells toward a pro-metastatic phenotype through MET. Nat Med 2012;18:883–91.
7. Herault A, Binnewies M, Leong S, Calero-Nieto FJ, Zhang SY, Kang YA, et al. Myeloid progenitor cluster formation drives emergency and leukemic myelopoiesis. Nature 2017;544:53–8.
8. Pietras EM, Mirantes-Barbeito C, Fong S, Loeffler D, Kovtonyuk LV, Zhang S, et al. Chronic interleukin-1 exposure drives hematopoietic stem cells towards precocious myeloid differentiation at the expense of self-renewal. Nat Cell Biol 2016;18:607–18.

9. Ueda Y, Cain DW, Kuraoka M, Kondo M, Kelsoe G. IL1R type I-dependent hemopoietic stem cell proliferation is necessary for inflammatory granulopoiesis and reactive neutrophilia. J Immunol 2009;182:6477–84.
10. Chiodoni C, Cancila V, Renzi TA, Perrone M, Tomirotti AM, Sangaletti S, et al. Transcriptional profiles and stromal changes reveal bone marrow adaptation to early breast cancer in association with deregulated circulating microRNAs. Cancer Res 2020;80:484–98.
11. Lara-Astiaso D, Weiner A, Lorenzo-Vivas E, Zaretsky I, Jaitin DA, David E, et al. Immunogenetics. Chromatin state dynamics during blood formation. Science 2014;345:943–9.
12. Maruyama K, Fukasaka M, Vandenbon A, Saitoh T, Kawasaki T, Kondo T, et al. The transcription factor Jdp2 controls bone homeostasis and antibacterial immunity by regulating osteoclast and neutrophil differentiation. Immunity 2012;37:1024–36.
13. Boggio K, Nicoletti G, Di CE, Cavallo F, Landuzzi L, Melani C, et al. Interleukin 12–mediated prevention of spontaneous mammary adenocarcinomas in two lines of Her-2/neu transgenic mice. J Exp Med 1998;188:589–96.
14. Lucchini F, Sacco MG, Hu N, Villa A, Brown J, Cesano L, et al. Early and multifocal tumors in breast, salivary, harderian and epididymal tissues developed in MMTY-Neu transgenic mice. Cancer Lett 1992;64:203–9.
15. Majorini MT, Cancila V, Rigoni A, Botti L, Dugo M, Triulzi T, et al. Infiltrating mast cell-mediated stimulation of estrogen receptor activity in breast cancer cells promotes the luminal phenotype. Cancer Res 2020;80:2311–24.
16. Tripodo C, Bassani B, Jachetti E, Cancila V, Chiodoni C, Portararo P, et al. Neutrophil extracellular traps arm DC vaccination against NPM-mutant myeloproliferation. Elife 2022;11:e69257.
17. Phipson B, Lee S, Majewski IJ, Alexander WS, Smyth GK. Robust hyperparameter estimation protects against hypervariable genes and improves power to detect differential expression. Ann Appl Stat 2016;10:946–63.
18. Giussani M, Ciniselli CM, De Cecco L, Lecchi M, Dugo M, Gargiuli C, et al. Circulating miRNAs as novel non-invasive biomarkers to aid the early diagnosis of suspicious breast lesions for which biopsy is recommended. Cancers 2021;13:4028.
19. Quaglino E, Mastini C, Forni G, Cavallo F. ErbB2 transgenic mice: a tool for investigation of the immune prevention and treatment of mammary carcinomas. Curr Protoc Immunol 2008;Chapter 20:Unit 20 9 1- 9–10.
20. Hai T, Wolfgang CD, Marsee DK, Allen AE, Sivaprasad U. ATF3 and stress responses. Gene Expr 1999;7:321–35.
21. Zambetti NA, Ping Z, Chen S, Kenswil KJG, Mylona MA, Sanders MA, et al. Mesenchymal inflammation drives genotoxic stress in hematopoietic stem cells and predicts disease evolution in human preleukemia. Cell Stem Cell 2016;19:613–27.
22. Wu Y, Campos L, Daguenet E, He Z, Picot T, Tavernier-Tardy E, et al. FAK deficiency in bone marrow stromal cells alters their homeostasis and drives abnormal proliferation and differentiation of hematopoietic stem cells. Cells 2020;9:646.
23. Ratajczak MZ, Bujko K, Cymer M, Thapa A, Adamiak M, Ratajczak J, et al. The Nlrp3 inflammasome as a "rising star" in studies of normal and malignant hematopoiesis. Leukemia 2020;34:1512–23.
24. Tamura T, Nagamura-Inoue T, Shmeltzer Z, Kuwata T, Ozato K. ICSBP directs bipotential myeloid progenitor cells to differentiate into mature macrophages. Immunity 2000;13:155–65.
25. Kurotaki D, Osato N, Nishiyama A, Yamamoto M, Ban T, Sato H, et al. Essential role of the IRF8-KLF4 transcription factor cascade in murine monocyte differentiation. Blood 2013;121:1839–49.
26. Gough PJ, Gordon S, Greaves DR. The use of human CD68 transcriptional regulatory sequences to direct high-level expression of class a scavenger receptor in macrophages *in vitro* and *in vivo*. Immunology 2001;103:351–61.
27. Lotti F, Menguzzato E, Rossi C, Naldini L, Ailles L, Mavilio F, et al. Transcriptional targeting of lentiviral vectors by long terminal repeat enhancer replacement. J Virol 2002;76:3996–4007.
28. Strobl H, Scheinecker C, Csmarits B, Majdic O, Knapp W. Flow cytometric analysis of intracellular CD68 molecule expression in normal and malignant hemopoiesis. Br J Haematol 1995;90:774–82.
29. LaBreche HG, Nevins JR, Huang E. Integrating factor analysis and a transgenic mouse model to reveal a peripheral blood predictor of breast tumors. BMC Med Genomics 2011;4:61.
30. Tcyganov EN, Hanabuchi S, Hashimoto A, Campbell D, Kar G, Slidel TW, et al. Distinct mechanisms govern populations of myeloid-derived suppressor cells in chronic viral infection and cancer. J Clin Invest 2021;131:e145971.
31. Strauss L, Sangaletti S, Consonni FM, Szebeni G, Morlacchi S, Totaro MG, et al. RORC1 regulates tumor-promoting "emergency" granulo-monocytopoiesis. Cancer Cell 2015;28:253–69.
32. Wolford CC, McConoughey SJ, Jalgaonkar SP, Leon M, Merchant AS, Dominick JL, et al. Transcription factor ATF3 links host adaptive response to breast cancer metastasis. J Clin Invest 2013;123:2893–906.
33. Ridker PM, MacFadyen JG, Thuren T, Everett BM, Libby P, Glynn RJ, et al. Effect of interleukin-1beta inhibition with canakinumab on incident lung cancer in patients with atherosclerosis: exploratory results from a randomized, double-blind, placebo-controlled trial. Lancet 2017;390:1833–42.
34. Wu TC, Xu K, Martinek J, Young RR, Banchereau R, George J, et al. IL1 receptor antagonist controls transcriptional signature of inflammation in patients with metastatic breast cancer. Cancer Res 2018;78:5243–58.